Assessment of Model Parameters in MFiX Particle-In-Cell Approach

Avinash Vaidheeswaran[a,b], Aytekin Gel[a,c], Mary Ann Clarke[a,b], William A. Rogers[a]

[a] *US Department of Energy, National Energy Technology Laboratory, 3610 Collins Ferry Rd, Morgantown, WV 26507*
[b] *LRST, 3610 Collins Ferry Rd, Morgantown, WV 26507*
[c] *ALPEMI Consulting, L.L.C., 8205 S. Priest Dr. # 13951, Tempe, AZ 85284*

Abstract

The limitations in numerical treatment of solids-phase in conventional methods like Discrete Element Model and Two-Fluid Model have facilitated the development of alternative techniques such as Particle-In-Cell (PIC). However, a number of parameters are involved in PIC due to its empiricism. In this work, global sensitivity analysis of PIC model parameters is performed under three distinct operating regimes common in chemical engineering applications, viz. settling bed, bubbling fluidized bed and circulating fluidized bed. Simulations were performed using the PIC method in Multiphase Flow with Interphase eXchanges (MFiX) developed by National Energy Technology Laboratory (NETL). A non-intrusive uncertainty quanti-

Email address: avinash.vaidheeswaran@netl.doe.gov (Avinash Vaidheeswaran)

cation (UQ) based approach is applied using Nodeworks to first construct an adequate surrogate model and then identify the most influential parameters in each case. This knowledge will aid in developing an effective design of experiments and determine optimal parameters through techniques such as deterministic or statistical calibration.

Keywords: Particle-In-Cell, Multiphase, MFiX, Nodeworks, Global Sensitivity Analysis, Sobol' Indices, Surrogate Modeling, Response Surface

1. Introduction

Coarse-grained Lagrangian techniques for representing particles in multiphase flow systems have been gaining significant attention over the past few years. In these systems, very large particle counts are re-imagined using a smaller number of particle clusters, thus reducing the overall number of Lagrangian entities to track in a simulation. Historically, solids modeling has been accomplished through Discrete Element Model (DEM) based on Lagrangian approach, or Two-Fluid Model (TFM) based on Eulerian approach. In a conventional DEM, every particle is represented individually and their interactions with neighbors are resolved. Consequently, simulations employing DEM may become intractable for pilot-scale or industrial-scale applications

where particle counts are very large. With recent advances in supercomputing architectures, efforts are currently underway to push the boundaries of conventional DEM Musser et al. [1], although the ease of availability of such resources is questionable at least in the near future. In TFM, solids are represented as a continuous phase. Simulations employing TFM are often prone to inaccuracies while modeling densely packed regions, where uncertainty is embedded in constitutive relations, like frictional models which do not model static regions well [2, 3, 4, 5]. The limitations of DEM and TFM have forced researchers to look for alternative methods to model multiphase flow systems having a large particle count. The development of coarse-grained strategies like Coarse-Grained DEM [6, 7, 8, 9] and Particle-In-Cell (PIC) [10, 11] are a consequence of this research.

PIC rests on the mathematical foundations laid by many researchers. Harlow and Welch [12] described PIC methodology for single-phase flows. Andrews and O'Rourke [13] formulated a one-dimensional PIC model for particle-laden flows. Snider and co-workers extended that work to two-dimensions [14], and later to three-dimensions [10]. More recent efforts to enhance multi-phase PIC modeling have focused on better management of physical mechanisms including formulations for collisional damping [15, 16],

collisional return to isotropy [17] and blended acceleration [18]. Scientific computational models developed by Snider and his co-workers have been built into the commercial software code, CPFD Barracuda®. Besides, a version of PIC called Dense Discrete Phase Model (DDPM) exists in Ansys Fluent®. Open-source PIC codes such as MFiX-PIC [19], [20] and MPPIC-Foam (OpenFOAM®) are also available.

In the majority of implementations, PIC relies on empiricism for modeling collisional stress [10, 21, 22] and the computational algorithm is not as straightforward compared to DEM. This warrants a rigorous analysis of its model parameters and numerical implementation. The current study is aimed at understanding the influence of PIC model parameters or control variables on response quantities. Three widely different flow conditions are chosen for analysis: settling bed, bubbling fluidized bed and circulating fluidized bed (CFB). The results obtained will help to identify optimal PIC model parameters following the procedure outlined by Gel et al. [23]. An initial demonstration of finding the optimal PIC model parameters with the aid of deterministic calibration for the case of settling bed can be found in Gel et al. [24].

The remainder of the article is organized as follows: In Section 2, an

overview of MFiX-PIC implementation is provided followed by description of cases in Section 3. Results from global sensitivity analysis and grid refinement study are presented in Sections 4 and 5. Finally, the conclusions and future work are discussed in Section 6.

2. Overview of MFiX-PIC

The fundamental assumption of PIC is that particles sharing the same physical properties can be grouped into computational parcels. Furthermore, the particles are assumed to be mono-dispersed within a given parcel. Figure 1 represents the flow field as viewed under DEM and PIC formalisms. Each component in the solids-phase is assigned a statistical weight, W_p, which defines the number of particles in a parcel. A different value of W_p could be used for each component, and hence the number of particles represented by a parcel could vary depending on size or density. The solution methodology in MFiX-PIC follows closely the work of Snider, D.M. [10]. The translational momentum equation for a parcel is given by the following equation [25, 24],

$$\frac{dU_i}{dt} = g_i + S_{mi} + \frac{1}{\epsilon_s \rho_s} \frac{\partial \tau_p}{\partial x_i}. \tag{1}$$

where, U_i and g_i are parcel velocity and acceleration due to gravity in the

coordinate direction i. ρ_s and ϵ_s represent density and volume fraction of solids. S_{mi} contains contributions from pressure gradient and drag given by [25],

$$S_{mi} = -\frac{dP_g}{dx_i}V + \beta_g V(U_{gi} - U_i) \tag{2}$$

where, V, β and U_{gi} represent volume of particle, interphase drag coefficient and velocity of gas-phase in the coordinate direction i. τ_p in Equation 1 is the inter-particle solids stress given by,

$$\tau_p = \frac{P_0 \epsilon_s^{\beta}}{\max[\epsilon_s^* - \epsilon_s, \delta(1 - \epsilon_s)]}. \tag{3}$$

Parameters P_0 and β are linear pressure scale factor and exponential factor. The parameter δ is a small number (10^{-7}) included to avoid numerical divergence. Subsequently, the parcel locations are updated using velocities as follows,

$$\frac{dx_i}{dt} = U_i. \tag{4}$$

The inclusion of inter-particle stress is not straightforward and could be described by the following pseudo-algorithm [24],

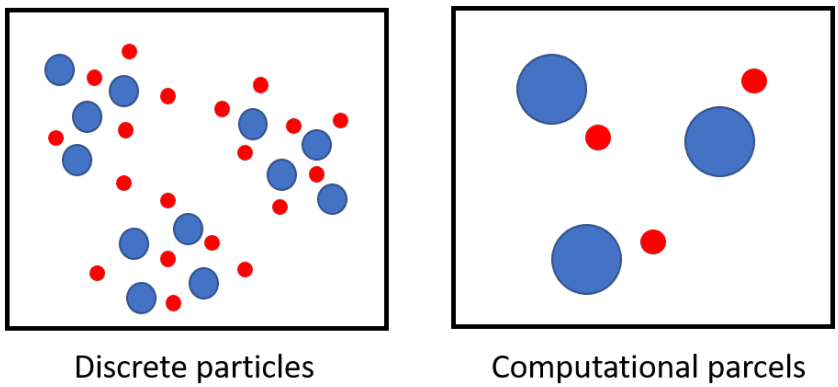

Figure 1: Visualization of discrete particles in DEM (left) and computational parcels in PIC (right).

if $\nabla\tau_p \leq 0$

PIC velocity contribution = min(δu_p,(1+γ)($\alpha\overline{U_p}$-$\tilde{u_p}$)

PIC velocity contribution = max(PIC velocity contribution,0)

else $\nabla\tau_p > 0$

PIC velocity contribution = max(δu_p,(1+γ)($\alpha\overline{U_p}$-$\tilde{u_p}$)

PIC velocity contribution = min(PIC velocity contribution,0)

endif

δu_p is the estimated discrete particle velocity contribution from inter-particle

stress. $\overline{U_p}$ and $\tilde{u_p}$ represent mean parcel velocity and parcel velocity evaluated without the stress term (Refer Equation 38 in Snider, D.M. [10]). γ is the elastic restitution factor whose default value is 0.85. A user-controlled factor, α, is applied to the solids slip velocity to account for local hydrodynamics.

Based on limited experience, P_0 is set in the range of [1-20]Pa for cases that are less dynamic like particles settling, and greater than 100Pa for cases having considerable particle motion like CFB. This could be visualized in a hypothetical flow regime map as shown in Figure 2. The x-axis represents the ratio of superficial velocity to minimum fluidization velocity, the latter being dependent on the properties of material and fluidizing medium. A rigorous approach is required for greater confidence in such hypothetical flow regime maps under different flow conditions. It must be noted that the collisional stress term has a multiplier (=10) in CPFD Barracuda®, and should be considered while comparing the values of P_0 used in MFiX-PIC while performing a code-to-code comparison. The parameter β is usually set to a value of 2-5. An appropriate value of statistical weight, W_p is not readily available in text, while it is believed among the developers of MFiX-PIC that the lower bound should not exceed 20 parcels/cell at close-packed conditions. It is typically advised to choose void fraction at close packing ϵ_s^*,

based on particle shape and size distribution, and the extent of polydispersity [26, 27, 28, 29, 30]. Finally, there is no body of literature to help select an appropriate value of α. A value of $\alpha = 0.5$ helped avoid excess over-packing while simulating a settling bed [20].

It is desired to provide the MFiX-PIC user community with a more specific range of values for the different model parameters. While this could be achieved through inverse techniques such as deterministic or Bayesian calibration, the first step is to determine sensitivity of model parameters, which is the focus of the work presented. In this study, global sensitivity analysis is used to rank model parameters and their interactive effects based on the order of importance under different flow conditions. This would also provide guidelines while designing simulation campaigns aimed at calibrating different model parameters.

The gas phase is treated as a continuum and modeled using the following continuity and momentum equations,

$$\frac{\partial}{\partial t}(\epsilon_g \rho_g) + \frac{\partial}{\partial x_j}(\epsilon_g \rho_g U_{gj}) = 0. \tag{5}$$

$$\frac{\partial}{\partial t}(\epsilon_g \rho_g U_{gi}) + \frac{\partial}{\partial x_j}(\epsilon_g \rho_g U_{gj} U_{gi}) = -\frac{\partial P_g}{\partial x_i} + \frac{\tau_{gij}}{\partial x_j} + \epsilon_g \rho_g g_i + S_{gi}. \qquad (6)$$

The terms P_g and τ_g represent pressure and shear stress in the gas phase. $S_{gi} = -\beta(U_{gi} - U_{mi})$, where U_{mi} is parcel velocity interpolated at cell center. Effects due to turbulence are not included in the current implementation of MFiX-PIC.

All the variables explored here are present in other PIC implementations such as CPFD Barracuda and MPPIC Foam except α. This has been exposed in MFiX-PIC as a user-controlled variable since the results were sensitive to its value at the time of testing. However, the findings from this study may not be extendable to DDPM in Ansys Fluent since the inter-particle collision stress is modeled using kinetic theory of granular flow (KTGF). Also, options based on kinetic theory exist for modeling particle interactions in CPFD Barracuda and MPPIC Foam where the analysis of variables in this study may not be applicable.

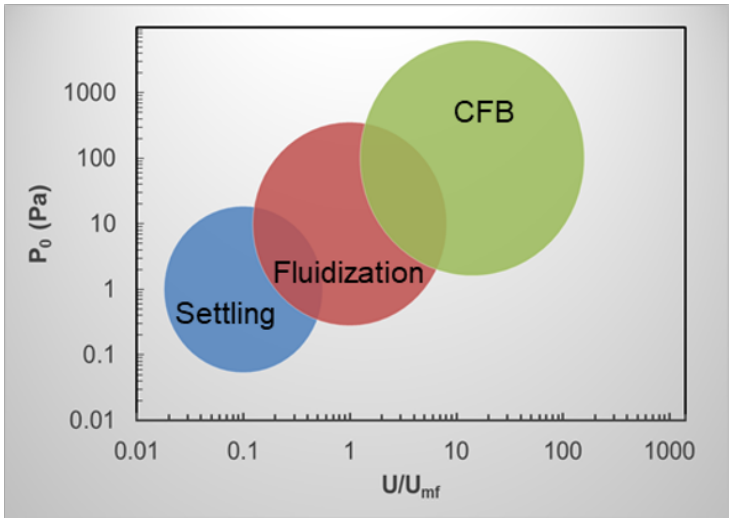

Figure 2: Hypothetical flow regime map [31]

	Pressure linear scale factor	Exponential factor	Statistical weight	Void fraction at max. packing	Solids slip velocity factor
Symbol	P_0	β	W_p	*epsilon**	α
Symbol in Nodeworks	t1	t2	t3	t4	t5
MFiX keyword	psfac_fric_pic	frix_exp_pic	ic_pic_const_statwt	ep_star	mppic_velfac_coeff
Range - Case 1	[1-20]	[2-5]	[3-8]	[0.35-0.5]	[0.5-1]
Range - Case 2	[1-100]	[2-5]	[10-100]	[0.4-0.5]	[0.85-0.98]
Range - Case 3	[1-250]	[2-5]	[3-60]	[0.35-0.5]	[0.85-0.98]

Table 1: Summary of PIC model parameters and their bounds for global sensitivity analysis

3. Description and Setup

Three different operating regimes are considered in this work to analyze the influence of PIC model parameters. Case 1, Case 2 and Case 3 correspond to a settling bed, a bubbling fluidized bed and a CFB respectively. Case 1 demonstrates particles settling in a dense medium, where $U/U_{mf} < 1$ is typically observed. The set-up used in this study is borrowed from the MFiX verification and validation manual [20] as depicted in Figure 3 and the preliminary results comparing MFiX-PIC, MFiX-TFM and MFiX-DEM are presented in Table 3. The range of parameters used in these simulations is summarized in Table 1. The grid size is set to 2mm in the three cartesian directions. A constant time step of 5×10^{-4}s is used, and the simulations are run for 1 second. The quantity of interest (QoI) is the location of filling shock whose analytical expression is given by,

$$y(t) = -t \left(\frac{\epsilon_s^* \epsilon_g^* u_r^* - \epsilon_{s0} \epsilon_{g0} u_{r0}}{\epsilon_s^* - \epsilon_{s0}} \right) \tag{7}$$

where, ϵ_s and u_r represent the volume fraction of solids-phase, volume fraction of gas-phase and the magnitude of relative velocity between the phases. Superscript '*' represents packed state and subscript '0' denotes values based

on initial conditions. Following Stokes' drag law, the relative velocity u_r is given by,

$$u_r = \frac{g\Delta\rho d_p^2}{18\mu_g}(1-\epsilon_s)^{3.65} \tag{8}$$

where, $g, \Delta\rho, d_p, \mu_g$ represent acceleration due to gravity, density difference, particle diameter and gas-phase viscosity. In this study, ϵ_{s0} is set to 0.15, and the analytical solution for the location of filling shock at the end of 1 second is 0.0751m. Nodeworks was used to generate 110 samples using the Latin Hypercube method optimized by the genetic algorithm of Jin et al. [32] as shown in the scatter plot matrix format of Figure 6. The Latin Hypercube method is preferred due to its space filling property, which can be qualitatively observed in the plots shown in Figure 6. The diagonal contains histograms of samples for each model parameter. The remaining tiles represent parity scatter plots between two given model parameters. For samples with good space-filling property, one would notice uniform distribution in the histograms and homogeneous space coverage in the off-diagonal plots.

Case 2 demonstrates bubbling fluidization based on the experiments of Vaidheeswaran et al. [33] and Vaidheeswaran and Rowan [34]. In this flow regime, bubbles or regions of void occur frequently in the emulsion phase.

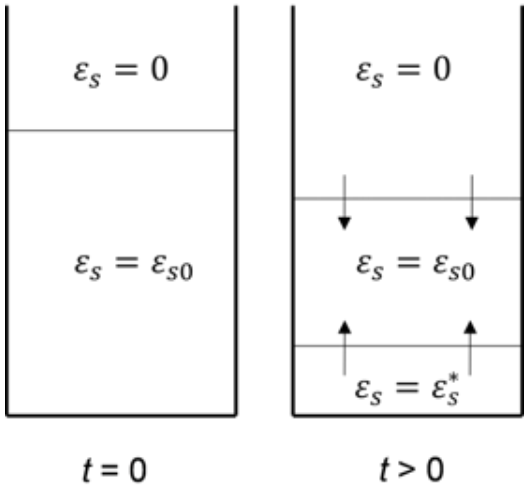

Figure 3: Schematic of settling bed in Case 1

	$\epsilon_{s0} = 0.10$	$\epsilon_{s0} = 0.15$	$\epsilon_{s0} = 0.20$
Analytical	0.466	0.544	0.607
MFiX-PIC	0.455 ± 0.01	0.521 ± 0.01	0.583 ± 0.01
MFiX-DEM	0.455 ± 0.01	0.515 ± 0.01	0.575 ± 0.01
MFiX-TFM	0.475 ± 0.01	0.555 ± 0.01	0.615 ± 0.01

Table 2: Preliminary results for the location of filling shock (in m) from Verification and Validation manual [20].

These bubbles erupt at the interface throwing particles on to the freeboard region. The flow rates in these systems are such that the solids do not elutriate out of the system, but instead return to the dense bed due to gravity. Typically, $U/U_{mf} > 1$, and the value used in this study is U/U_{mf} =2.97. The computational domain, which is a cylindrical unit having an internal diameter of 2.5" (6.35cm) is a simplified representation of the actual unit used in the experiments. A rough schematic including the location of pressure sensors is shown in Figure 4. The range of parameters used in these simulations is summarized in Table 1. The grid size is set to 3.33mm in the three cartesian directions. A variable time step is used, having a maximum value of 5×10^{-4}s, and the simulations are run for 50 seconds. A total of 110 sampling locations were generated using the Latin Hypercube method in Nodeworks optimized with the genetic algorithm of Jin et al. [32] as shown in Figure 7.

Case 3 demonstrates a CFB based on the experiments of Xu et al. [35] whose schematic is shown in Figure 5. The riser has a height of 1.32m, and the internal diameters of cyclone, riser and standpipe are 0.127m, 0.0508m and 0.0254m. Air enters through flow controllers FTC180, FTC135 and FTC115. The flow rates used in this study are 300, 7 and 2.5 standard liter per minute (SLPM). This translates to a velocity of 2.46m/s at the bottom

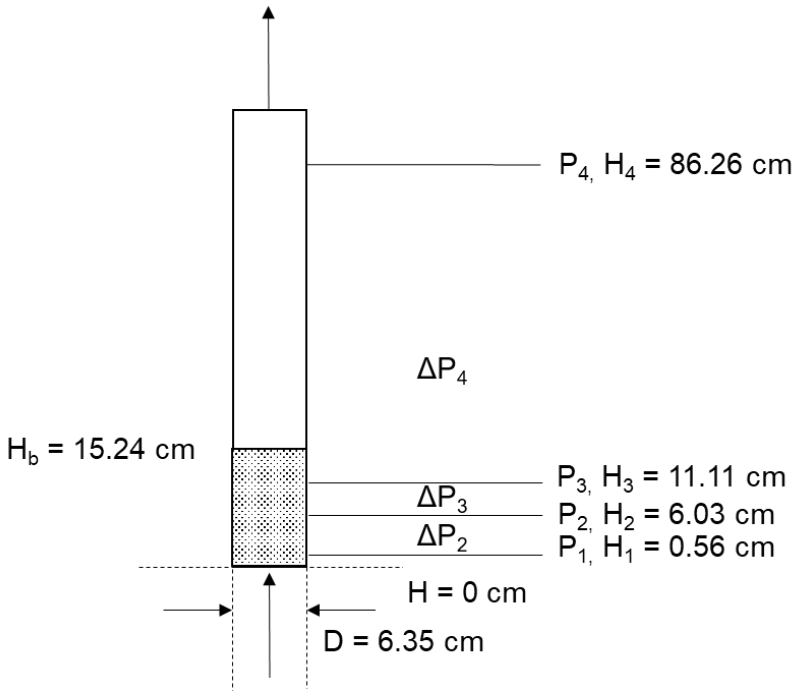

Figure 4: Set up of bubbling fluidized bed in Case 2.

of the riser and the corresponding U/U_{mf} is more than 10. This ratio is significantly higher than the bubbling fluidized bed (Case 2). The range of parameters used in these simulations is summarized in Table 1. The grid size is set to 5mm in the three cartesian directions. A variable time step is used, having a maximum value of 5×10^{-4}s, and the simulations are run for 45 seconds. A total of 110 sampling locations were generated using the Latin Hypercube method in Nodeworks optimized with the genetic algorithm of Jin et al. [32] as shown in Figure 8.

The open-source scientific workflow Nodeworks (version 20.2) [36] was used for non-simulation tasks, i.e., design of experiments (DOE), surrogate model construction and sensitivity analysis. Nodeworks provides a framework for GUI based programming using nodes and connections as shown in Figure 9. A logical workflow was established wherein the DOE was generated followed by a simulation campaign and then sensitivity analysis performed with the QoIs from the simulation campaigns. Simulations were performed using MFiX-20.1 [37]. Results from the simulation campaigns were post-processed and provided as externally generated tabulated input to Nodeworks for sensitivity analysis. The method of Sobol' indices [38] was used to quantify the influence of model parameters on the observed QoIs.

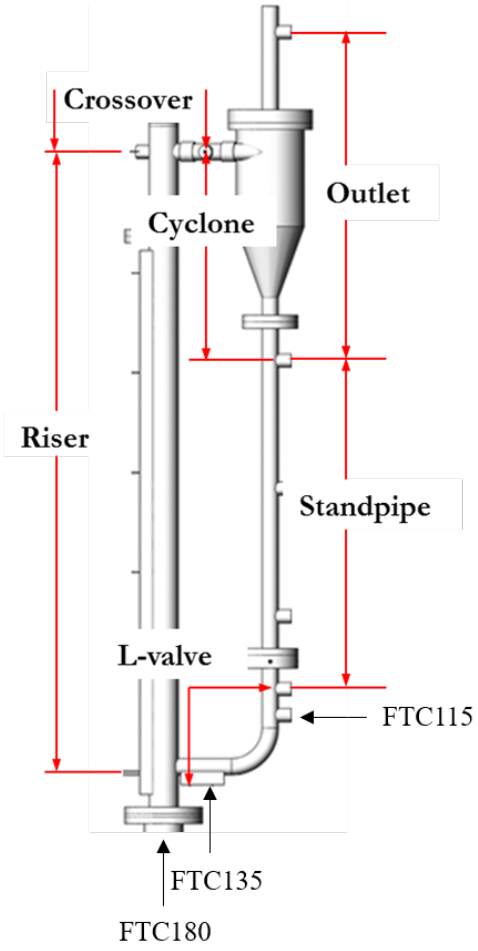

Figure 5: Setup of circulating fluidized bed in Case 3.

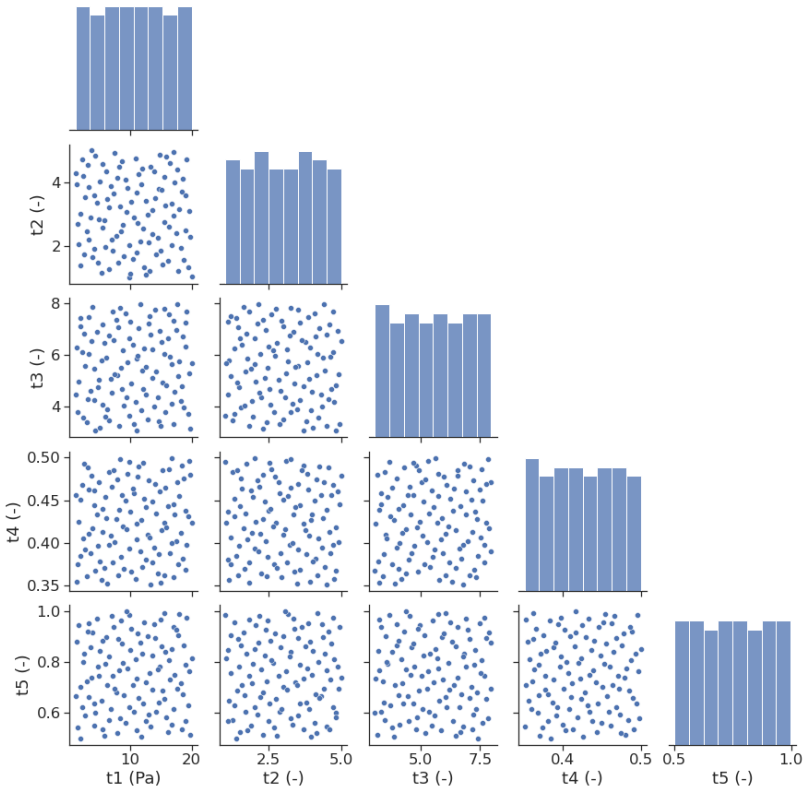

Figure 6: Scatter plot matrix showing 110 samples in the simulation campaign generated for Case 1. Histograms along the diagonal represent uniform distribution of model parameters.

4. Global Sensitivity Analysis

4.1. Case 1: Particles settling in a dense medium

MFiX-PIC simulations were performed at the sampling locations given in Figure 6. At the end of 1 second, slices of line-averaged gas volume fraction were extracted to determine the location of filling shock. The threshold value

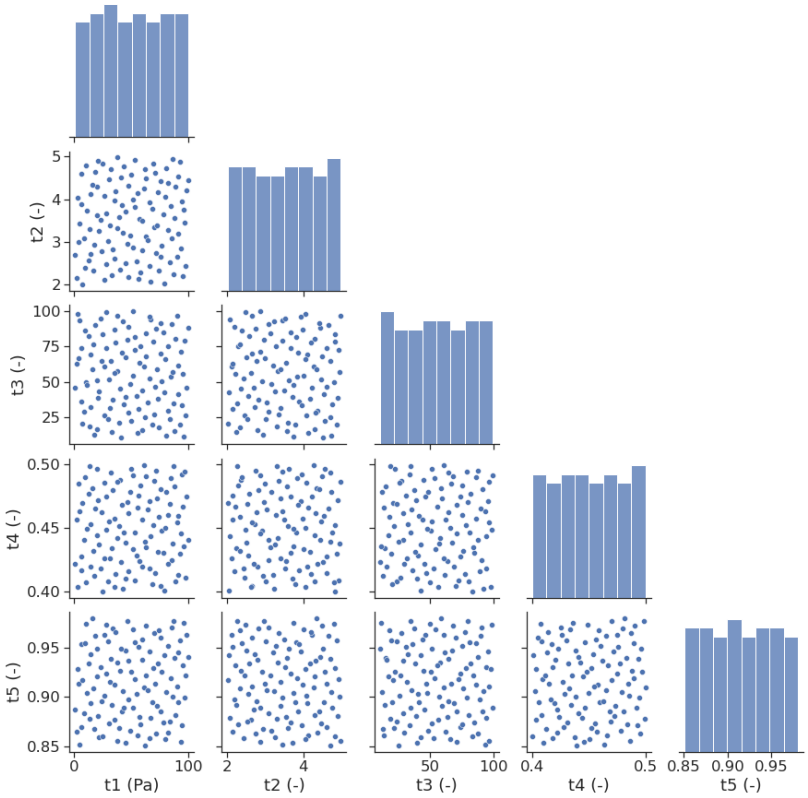

Figure 7: Scatter plot matrix showing 110 samples in the simulation campaign generated for Case 2. Histograms along the diagonal represent uniform distribution of model parameters.

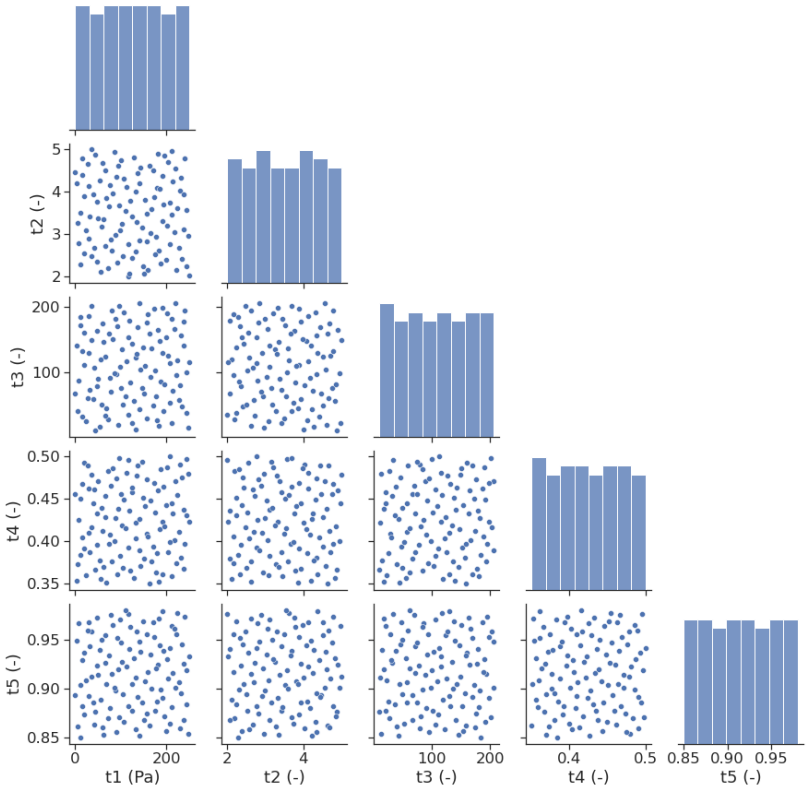

Figure 8: Scatter plot matrix showing 110 samples in the simulation campaign generated for Case 3. Histograms along the diagonal represent uniform distribution of model parameters.

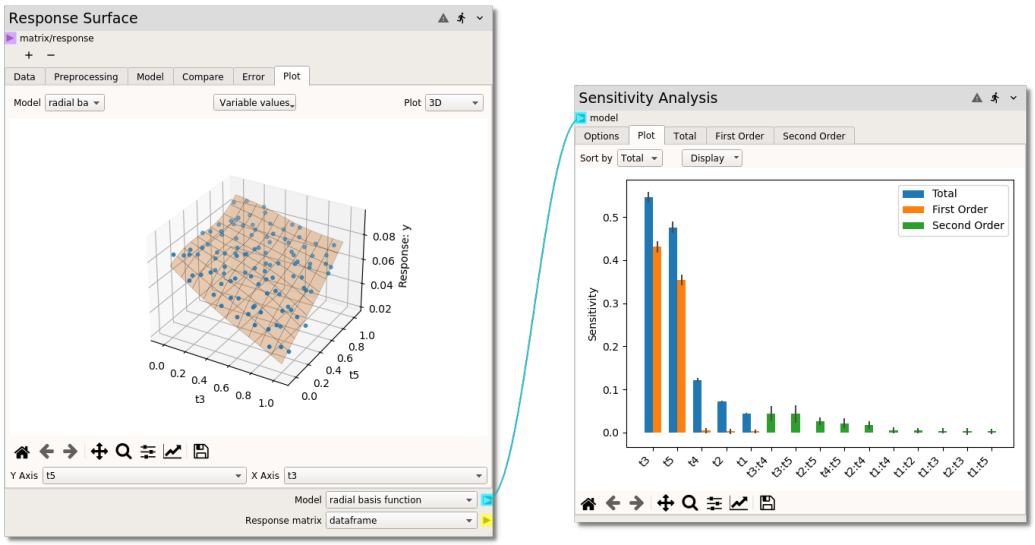

Figure 9: Snapshot of Nodeworks workflow showing response surface and sensitivity analysis nodes for Case 1.

chosen was the average of gas volume fraction at maximum packing, ϵ_g^* and initial volume fraction of gas, ϵ_{g0}. The shock is assumed to be present at the first instance when volume fraction at a given vertical location is less than this average value. Figure 10 shows model parameters (considered as input variables) and the QoI obtained from the simulation campaign in the form of scatter plot matrix. The QoI is observed to decrease with increase in statistical weight (t3) while the opposite is true for solids slip velocity factor (t5). Different surrogate models were tested for the QoI, and radial basis functions (RBFs) provide an adequate description of overall behavior as observed through the mean squared error (MSE) and parity plot shown in Figure 11. The acronyms MLP, SVM and GPM refer to multi-layer perceptron, support vector machine and Gaussian process model respectively. The response surface constructed using RBFs in t3-t5 parameter space is shown in Figure 12. t1, t2 and t4 are set to the midpoint of their ranges while visualizing. The location of blue dots (results from simulations) need not necessarily overlap with the surface, however it could be seen that most of the variation in the QoI could be captured using t3 and t5.

The influence of model parameters is quantified using Sobol' Indices based sensitivity analysis method [38] as shown in Figure 13. Vertical bars indi-

cate the 95% confidence interval. The plot shows first order (main effects), second order (interactive effects) and total indices. t3 and t5 are observed to have the most dominant effect on the location of filling shock. Effects due to interactions between model parameters are present, however they are considerably less compared to main effects.

At this point it is not clear if statistical weight (t3) could be considered independent of grid discretization. Having a parcel volume comparable to or greater than the volume of an Eulerian cell would make interpolation questionable. Also, if the entire cell is packed by a single parcel, the inter-particle stress term becomes artificially high which might cause results to be erroneous. In this case, the maximum value of t3 is chosen such that the ratio of volume of parcel to volume of cell is 0.56 compared to the maximum solids concentration at packing (0.64). Hence, the latter situation could be avoided. However, the effect of parcel volume on the interpolation operation is yet to be determined.

The influence of solids slip velocity factor (t5) could be explained as follows; when t5 is 1, it is equivalent to having unimpeded relative motion between a parcel and its neighbors. This might be the case in regions having lower particle concentration or in the vicinity of a wall, where a parcel moves

relative to a stationary boundary. As concentration increases, a parcel's motion is influenced by its neighbors. Particles also have a tendency to move as clusters and their relative motion is reduced. In such instances, it is intuitive that the solids slip velocity factor is less than 1. This acts as a numerical limiter on the overall solids velocity and as t5 reduces, the location of filling shock moves lower in the domain. Finally, it must be emphasized that the observed trends are valid for the given range of model parameters, operating conditions and grid discretization. A more rigorous study is necessary to elucidate such effects and will be pursued in the future.

4.2. Case 2: Bubbling fluidized bed

MFiX-PIC simulations were performed at sampling locations shown in Figure 7. There were three QoIs, i.e., time-averaged ΔP_2, ΔP_3 and ΔP_4 calculated from the time series of pressure signals after removing the first 25 seconds to eliminate the effect of flow transients. These are referred to as DP2, DP3 and DP4 respectively due to typesetting inconsistencies in Nodeworks. The results are shown in the form of a scatter plot matrix in Figure 14, where a few qualitative trends emerge. There is a predominant inverse correlation between void fraction at maximum packing, t4 and the QoIs. DP2 and DP3 are proportional for the most part, which is to be

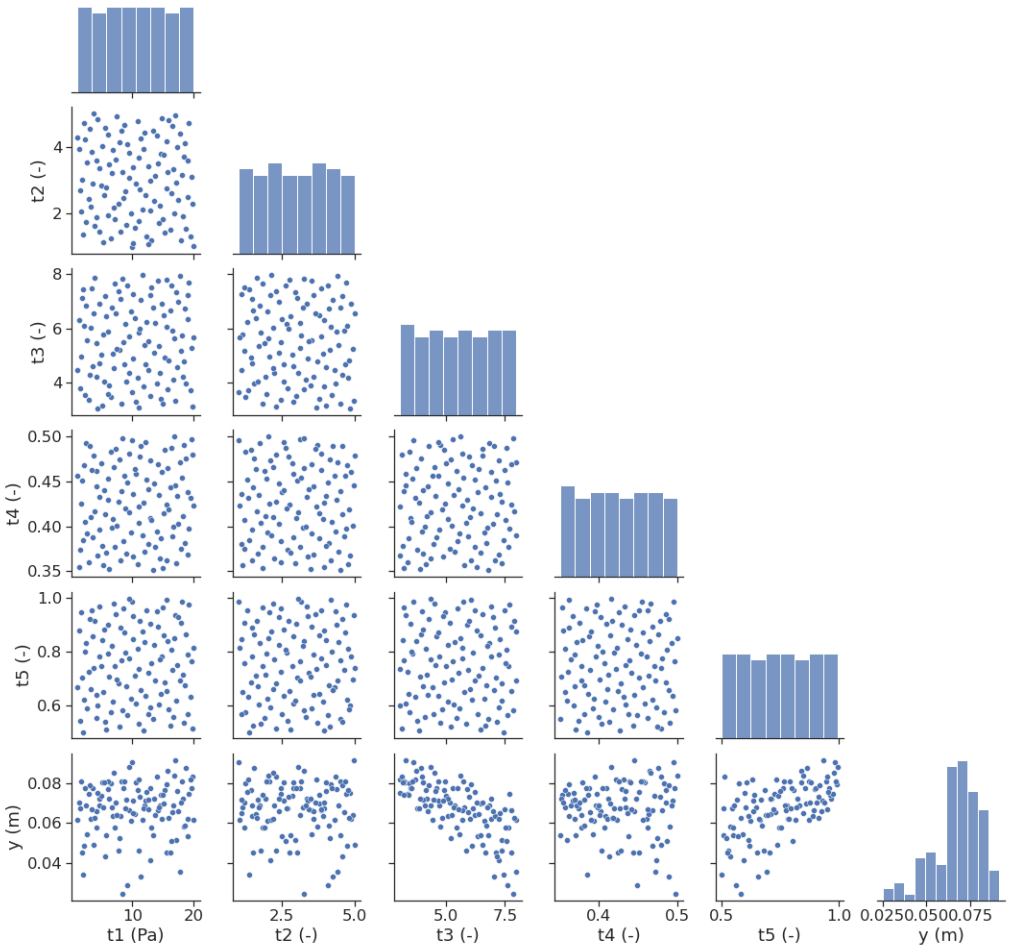

Figure 10: Scatter plot matrix showing model parameters along with the QoI in Case 1.

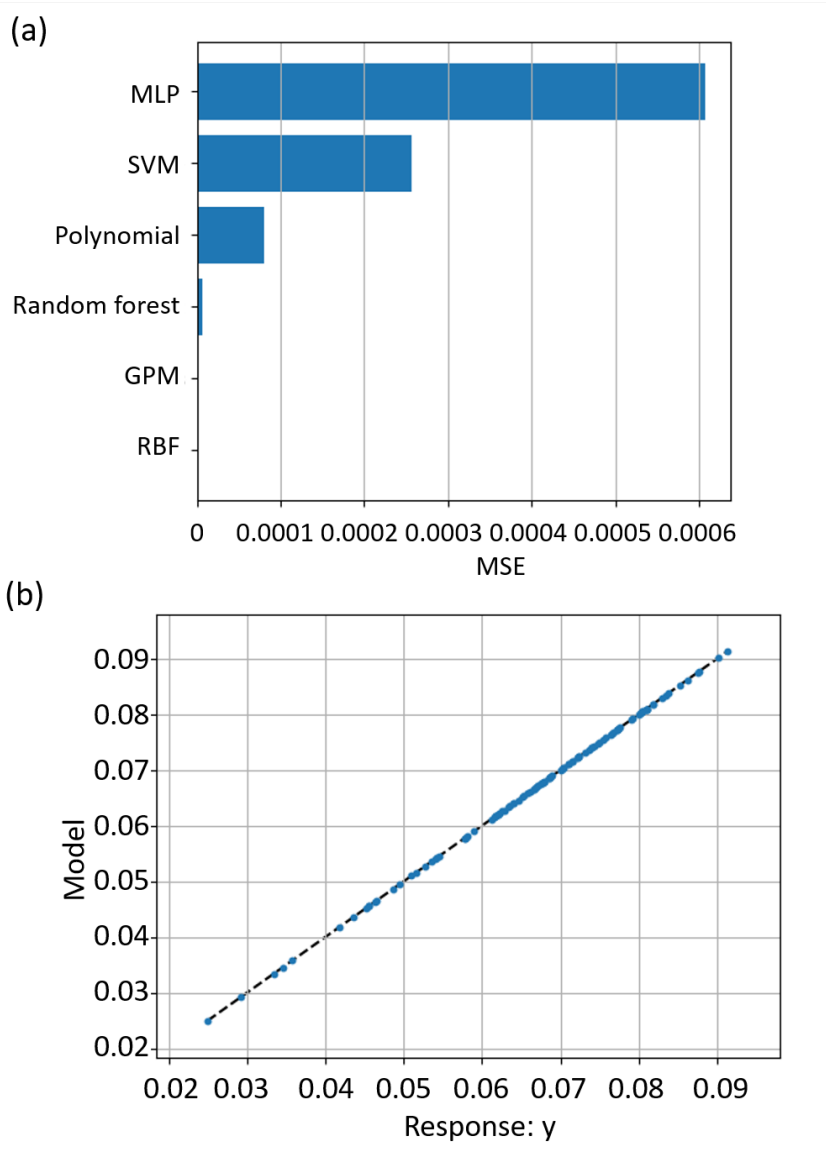

Figure 11: MSE calculated using different surrogate models (top), and parity plot for RBFs comparing the actual and predicted values (bottom) in Case 1.

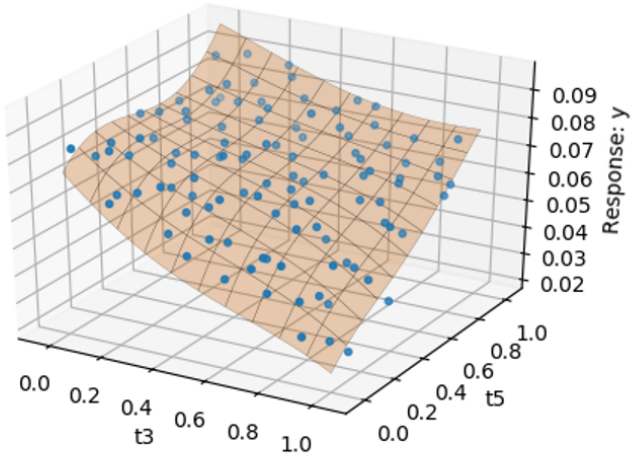

Figure 12: Response surface generated using RBFs for Case 1. Blue dots represent the actual location of samples in t3-t5 parameter space, while remaining input parameters (t1,t2,t4) are set to midpoint of their ranges.

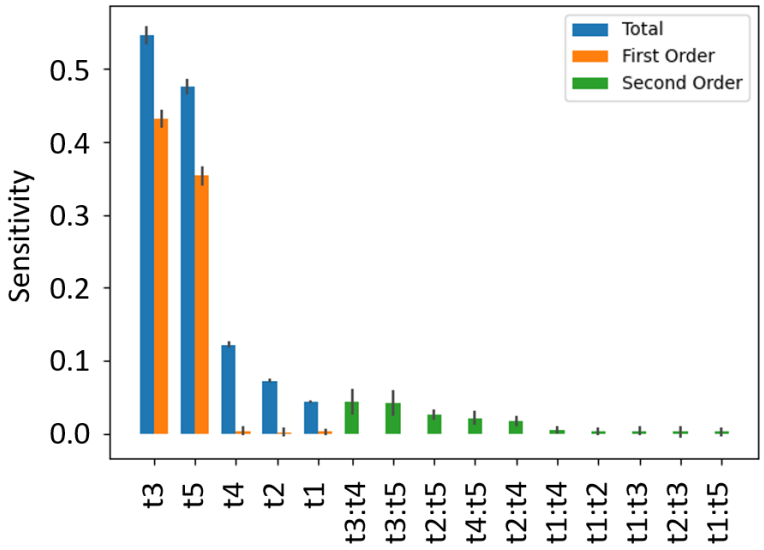

Figure 13: Sobol' indices computed using RBF based surrogate model for Case 1.

expected since their measurements were made in dense regions. The flow section corresponding to DP4 consists of both dense and dilute regions, and the time-averaged value shows a different behavior. As noticed previously, RBFs provide an adequate description of the overall behavior as seen from their MSE values and parity plots (Figure 15).

The parametric sensitivities are quantified using the method of Sobol' [38]. As expected, DP2 and DP3 are strongly influenced by t4, whose first-order Sobol' index is significantly higher than other first-order and second-order indices. For practical interpretation, t4 determines the amount of solids

being packed in a given cell besides appearing in the expression for inter-particle stress in the PIC model. As t4 increases, solids concentration in a given cell drops, which leads to a lower solids hold-up in dense regions. Pressure drop is determined by the weight of solids in these regions and hence, DP2 and DP3 decrease as t4 increases. However, DP4 is sensitive to changes in pressure linear scale factor, t1 and exponential factor, t2 besides t4. As solids concentration becomes more dilute, contributions from other model parameters become non-trivial. It may not be possible to associate all the observed parametric sensitivities with flow physics due to inherent empiricism in the PIC methodology.

4.3. Case 3: Circulating fluidized bed

MFiX-PIC simulations were performed for Case 3 at the sampling locations shown in Figure 8. The chosen QoIs were interface height (y1), pressure drop in riser (y2) and pressure drop in standpipe (y3). Time-averaged quantities are calculated from the corresponding time series after removing the first 25 seconds to eliminate the effect of flow transients. Interface height is determined as the point where the local ϵ_g exceeds 0.45 and the difference in ϵ_g between the adjacent cells in the vertical direction is greater than 0.05. Though the method used to determine y1 may be ad hoc, the QoI was ob-

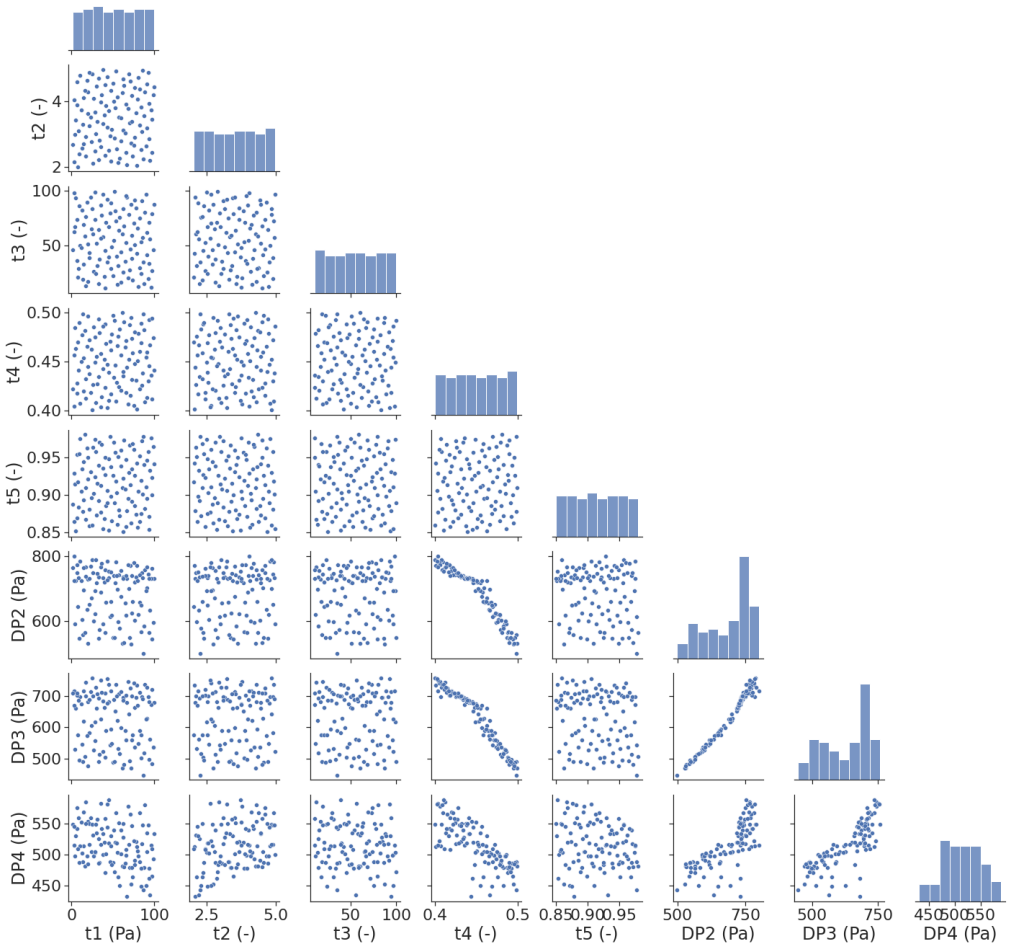

Figure 14: Scatter plot matrix showing model parameters along with the QoIs in Case 2.

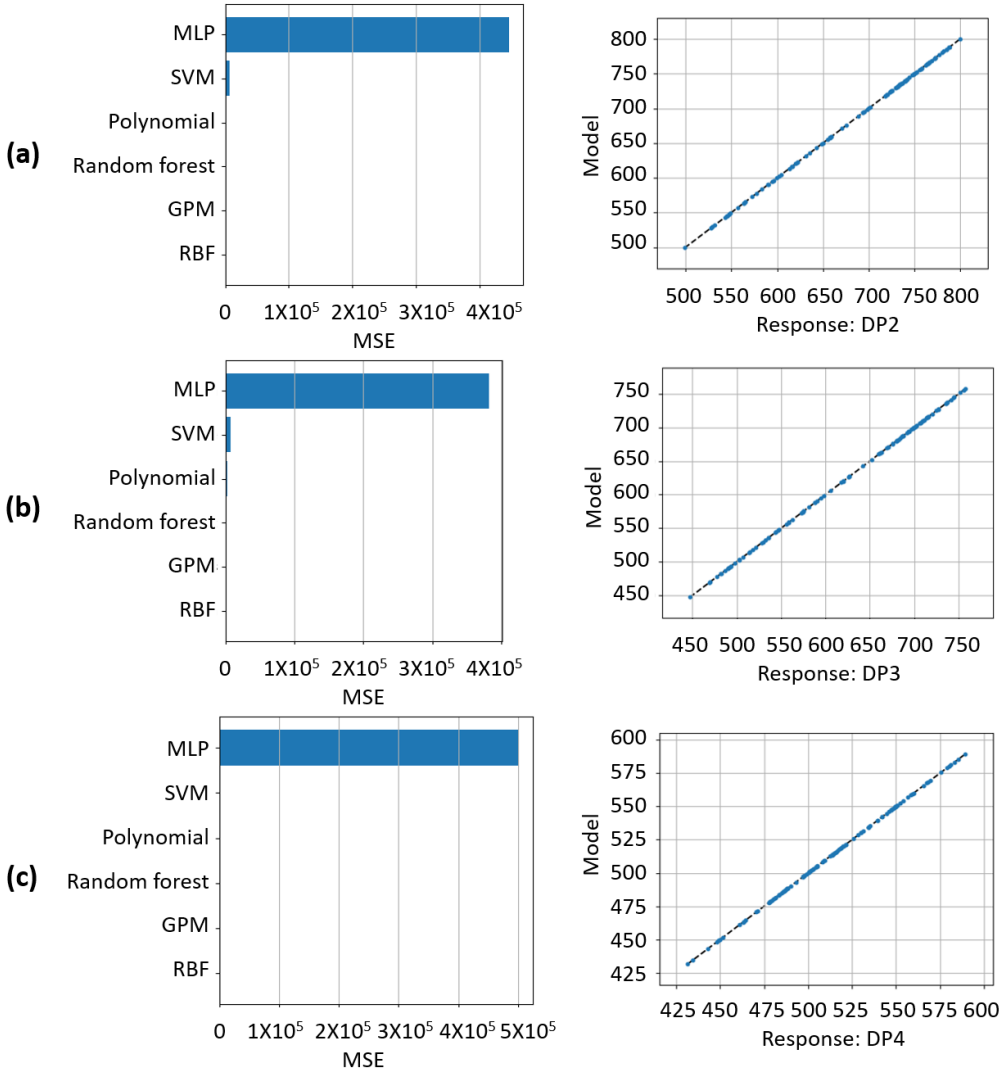

Figure 15: MSE plots (top) and parity plots (bottom) corresponding to (a) DP2, (b) DP3 and (c) DP4 in Case 2. Parity plots are shown for RBFs.

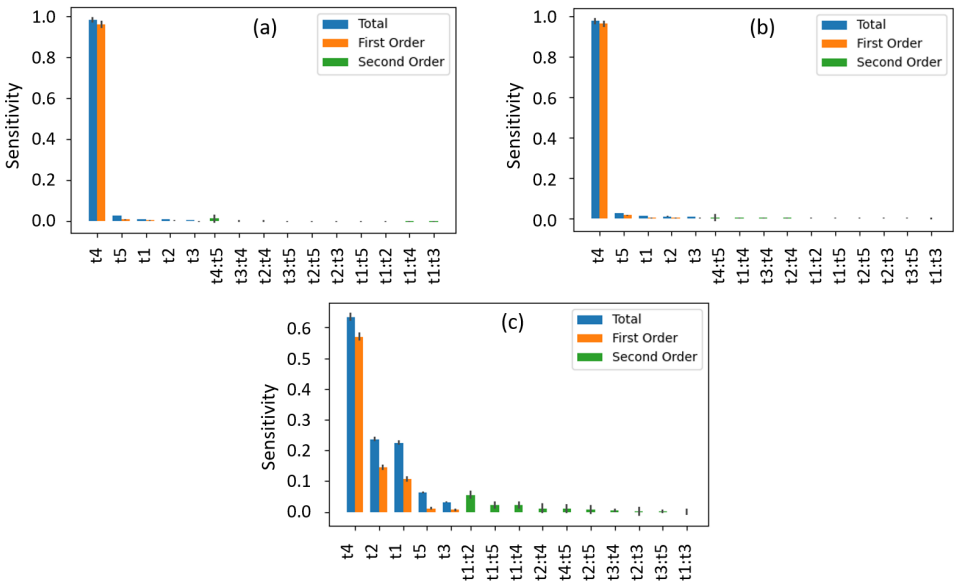

Figure 16: Sobol' indices computed using RBF based surrogate model for (a) DP2, (b) DP3 and (c) DP4 in Case 2:

served not to be sensitive to the threshold values owing to a sharp ϵ_g gradient at the interface. The results along with sampling locations are shown in the form of a scatter plot matrix in Figure 17. Some distinct trends are seen for parameters t3 and t4. y1 appears to drop slowly with an increase in t3 followed by a rapid decline towards the maximum limit, while y1 increases gradually with increase in t4, which determines the amount of solids that could be packed in a given region. The latter decreases and the interface height drops with increase in t4. Also, there is an overall drop in y2 and y3 with increase in t3 and t4.

Again RBFs were chosen for generating response surfaces after comparing the MSE values from different options in Nodeworks (Figure 18). The parity plot based on RBFs shows an accurate match between the observed and predicted values. These were used to perform function evaluations of the QoIs to compute the first order, second order and total indices shown in Figure 19. It is important to note that y1 (interface height) is sensitive to the interaction effects, i.e., combinations, besides first-order effects due to t3, t4 and t5. Overall, statistical weight, t3, seems to be the most influential parameter considering both the first order and second-order effects. y2 (pressure drop across riser) seems to have similar sensitivity to parameters t3, t4 and t5 while

y3 (pressure drop across standpipe) is very sensitive to t4 compared to other parameters. Influence of parametric interactions is slightly different between the two, but the magnitude of their indices suggests negligible sensitivities for y2 and y3. Case 3 consists of features from Case 1 and Case 2. The standpipe has a dense region where frictional contact is dominant, and the relative motion of solids is considerably less as observed for particles settling in a dense medium. On the other hand, the lower portion of the riser behaves as a fluidized bed albeit at a much higher velocity.

5. Effect of grid refinement

Finally, a grid refinement study was performed to assess the effect of grid resolution on Sobol' indices and order of ranking. First, Case 1 was analyzed using three different grid sizes: G_1^1-fine grid (2mm), G_2^1-intermediate grid (2.86mm) and G_3^1-coarse grid (4mm). The refinement ratio is more than 1.3 as recommended by Freitas [39]. As pointed out earlier, it is intuitive that the influence of statistical weight, t3, on the observed QoI might be correlated with grid size. Two different approaches were followed: (i) the same set of model parameters was used at each grid level, (ii) the range of t3 was modified based on cell volume while other parameters were held constant. In

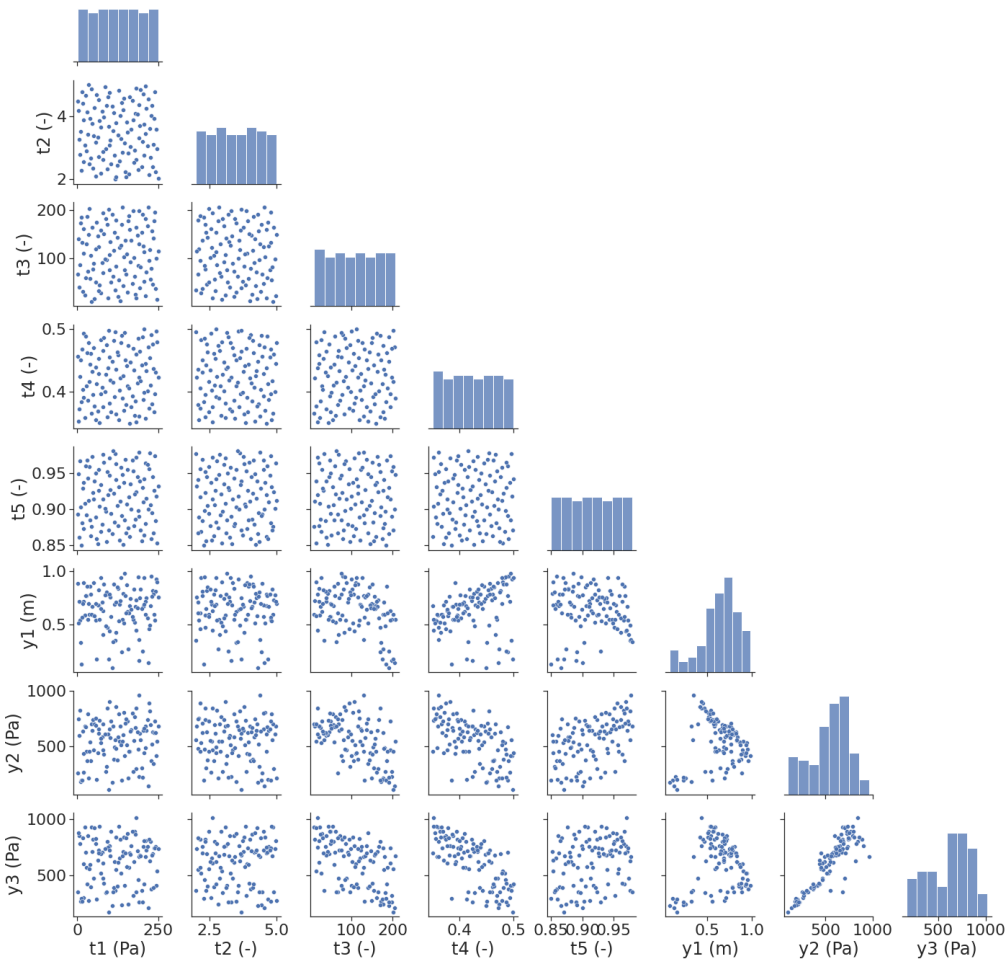

Figure 17: Scatter plot matrix showing model parameters along with the QoIs in Case 3.

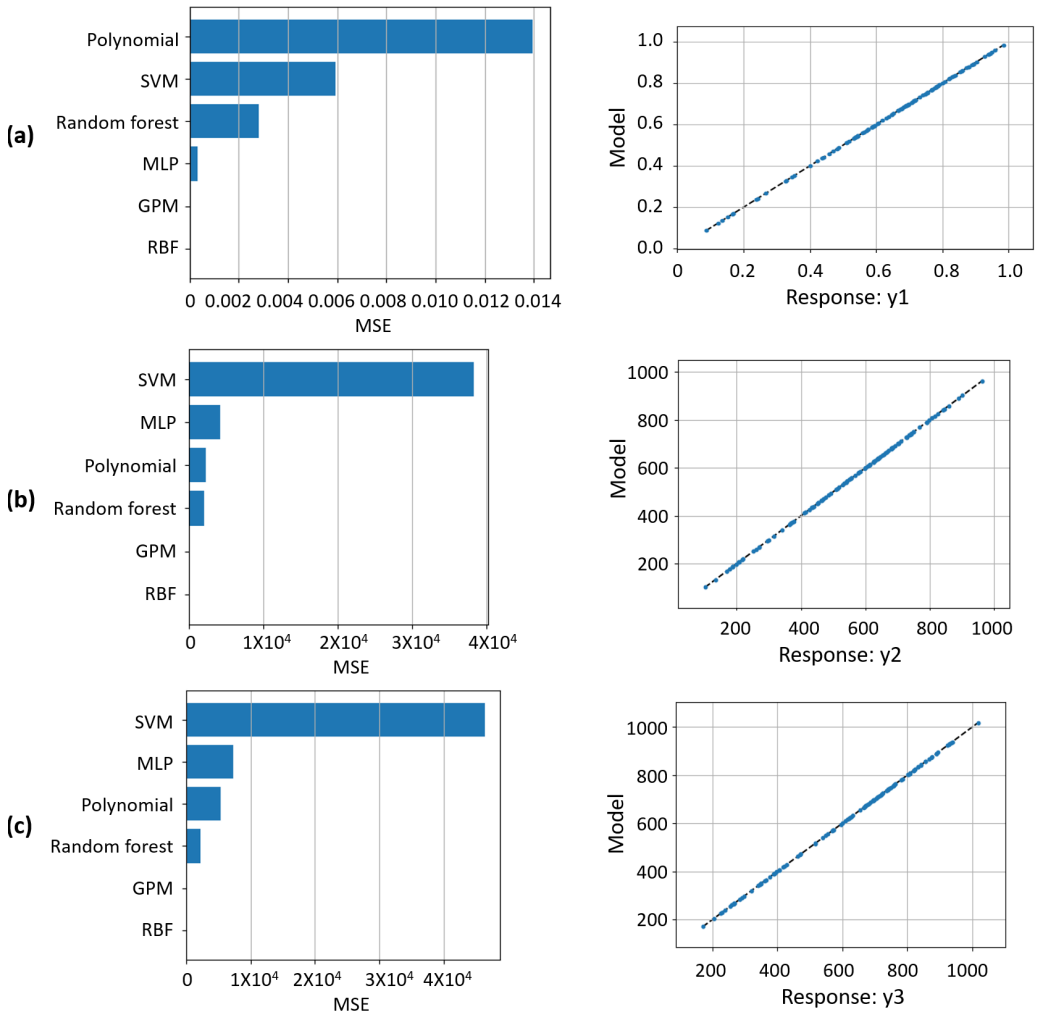

Figure 18: MSE (top) and parity plots (bottom) corresponding to (a) y1 (interface height in standpipe), (b) y2 (pressure drop across riser) and (c) y3 (pressure drop across standpipe) in Case 3. Parity plots are shown for RBFs.

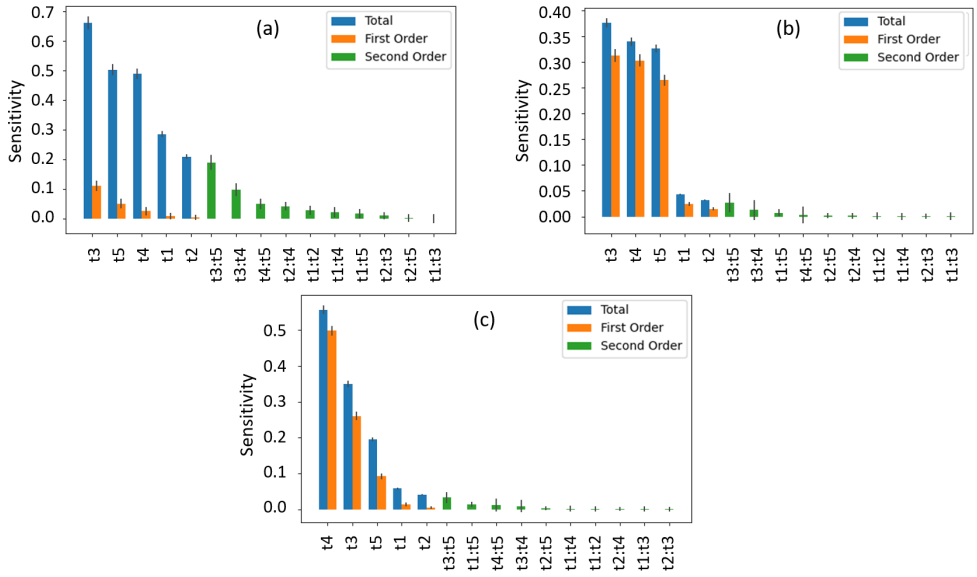

Figure 19: Sobol' indices computed using RBF based surrogate model for (a) y1 (Interface height in standpipe), (b) y2 (Pressure drop across riser) and (c) y3 (Pressure drop across standpipe) in Case 3.

Approach	$G_1^1(\Delta = 2mm)$	$G_2^1(\Delta = 2.86mm)$	$G_3^1(\Delta = 4mm)$
(i)	[3.00,8.00]	[3.00,8.00]	[3.00,8.00]
(ii)	[3.00,8.00]	[8.90,23.29]	[24.35,63.73]

Table 3: Range of t3 considered for DOE at different grid levels in Case 1.

approach (ii), the bounds for t3 at a given grid discretization are obtained by multiplying the bounds from the previous level with the ratio of grid volumes between the two (e.g., a factor of 2.92 was used obtained by $2.8^3/2^3$ between intermediate and fine grids). As a consequence, the maximum number of parcels per cell in G_1^1, G_2^1 and G_3^1 grids is determined only by volume fraction at maximum packing, t4, at a given sampling location in approach (ii). The bounds of t3 used at each level are summarized in Table 5.

Figure 20 presents a summary of results obtained using the two approaches. It can be seen clearly that the order of ranking remains consistent when t3 was scaled proportional to grid size, as opposed to preserving its original minimum and maximum bounds. Also, the magnitude of Sobol' indices are identical between G_1^1 and G_2^1 suggesting that the key model parameters affecting the variability observed in the QoI are consistent at both grid resolutions.

This procedure (approach (ii)) was used for Case 2 and Case 3, where the bounds for t3 are provided in Table 5. Figure 21 summarizes results from

Case 2		Case 3	
$G_1^2(\Delta = 3.33mm)$	[3.00,100.00]	$G_1^3(\Delta = 3.30mm)$	[3.00,60.00]
$G_2^2(\Delta = 5.18mm)$	[11.24,374.51]	$G_2^3(\Delta = 5.00mm)$	[10.32,206.34]

Table 4: Range of t3 considered for DOE at different grid levels in Case 2 and Case 3.

Case 2 using G_1^2-fine grid (3.33mm) and G_2^2-coarse grid (5.18mm). As noticed before, all QoIs are sensitive to void fraction at maximum packing (t4). The order of ranking is preserved for DP2 and DP3 with regards to the two most dominant parameters, t4 and t5, while only t4 is consistently predicted as the most dominant parameter for DP4. The magnitude of Sobol' indices corresponding to other parameters are much smaller or negligible compared to t4. One may not observe convergence in the order of ranking, but the most dominant parameter was identified as t4 consistently. The observed behavior could be due to lack of grid independence and further refinement may be needed.

Figure 22 summarizes results from Case 3 using G_1^3-fine grid (3.33mm) and G_2^3-coarse grid (5mm). The ranges used for t3 are provided in Table 5. As noticed before, interactive effects are dominant for y1, while being negligible for y2 and y3 at both the grid discretization levels. The order of ranking based on Sobol' indices and their magnitudes are consistently predicted for y2 and y3. This is not the case for y1 where significant deviation

is present, especially with pronounced effects of interaction between t3 & t4, and t3 & t5. This could possibly indicate lack of grid independence and finer resolution may be needed. Overall it could be concluded that scaling t3 while refining the grid appears to be more consistent with PIC methodology, however convergence was not demonstrated for all cases in the current analysis using this approach.

6. Conclusions and Future Work

Three distinct cases viz., settling bed, bubbling fluidized bed and CFB were selected to understand the influence of MFiX-PIC model parameters under different flow conditions. RBF based surrogate models constructed with the simulation campaign results were determined to characterize the relationship between the five model parameters and QoIs in each case.

The QoI in Case 1 was the location of filling shock which was mostly sensitive to statistical weight, t3 and solids slip velocity factor, t5. The effects of interaction among parameters (second-order effects) were negligible. In Case 2, DP2, DP3 and DP4 were the QoIs of which the first two were measured in dense regions while DP4 was measured in a combination of dense and dilute regions.DP2 and DP3 were strongly influenced by void fraction at

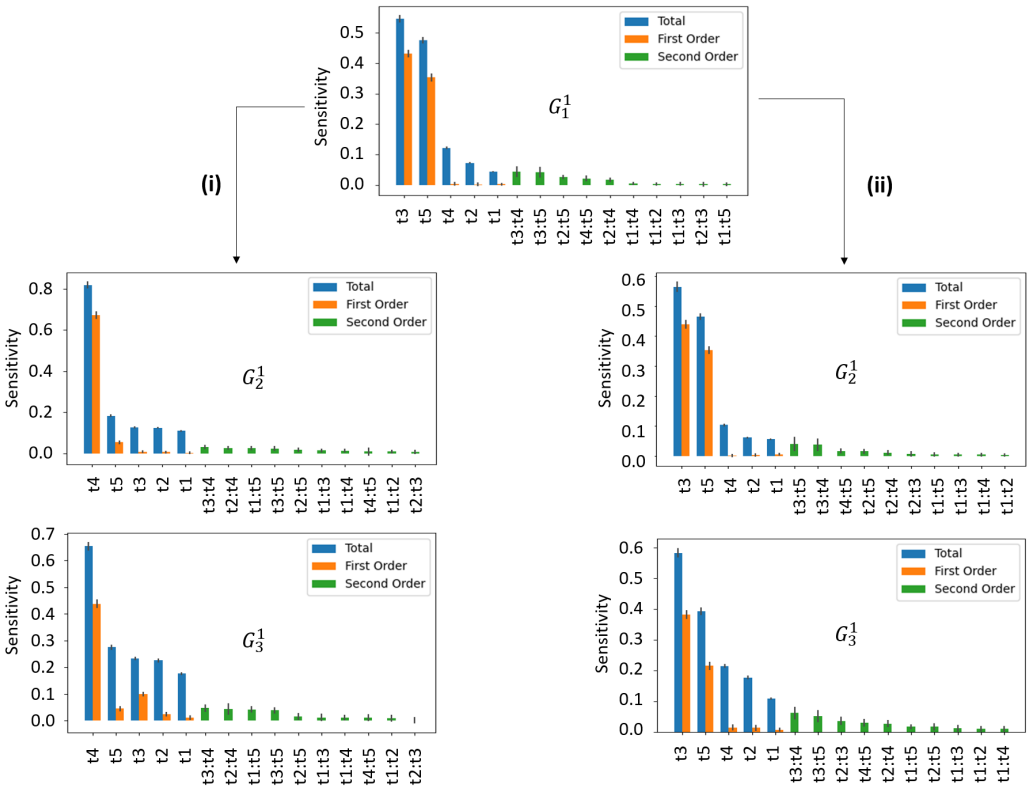

Figure 20: Effect of grid discretization on the order of ranking based on Sobol' indices for Case 1.

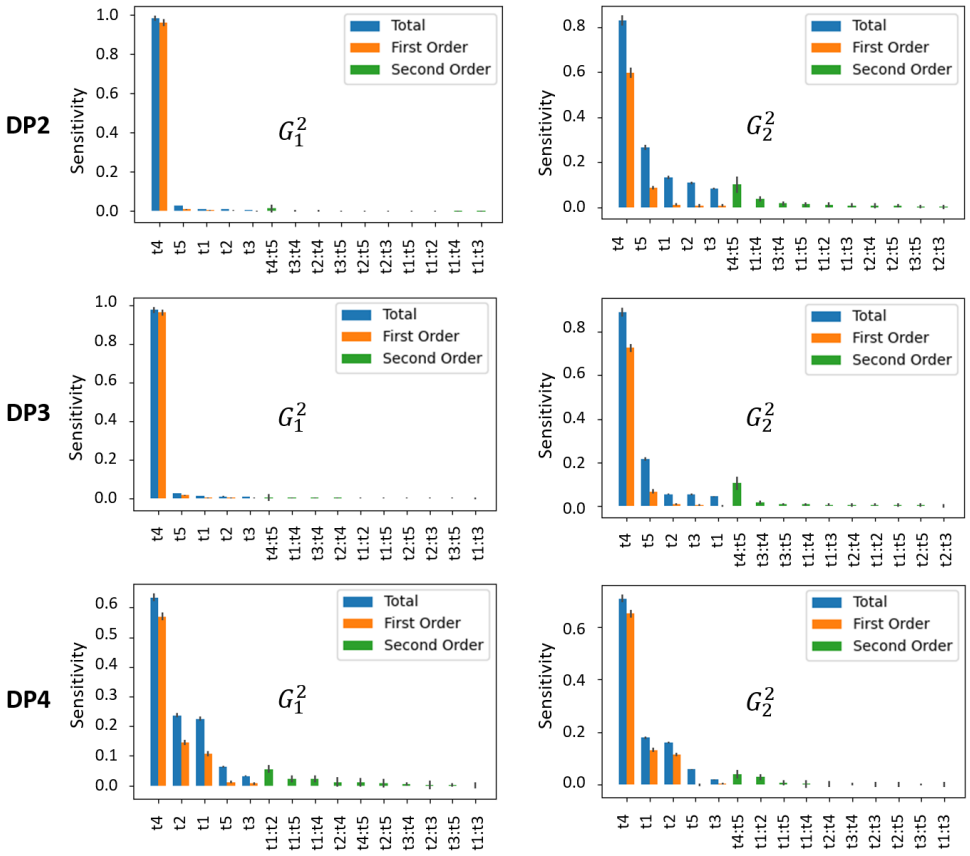

Figure 21: Effect of grid discretization on the order of ranking based on Sobol' indices for Case 2.

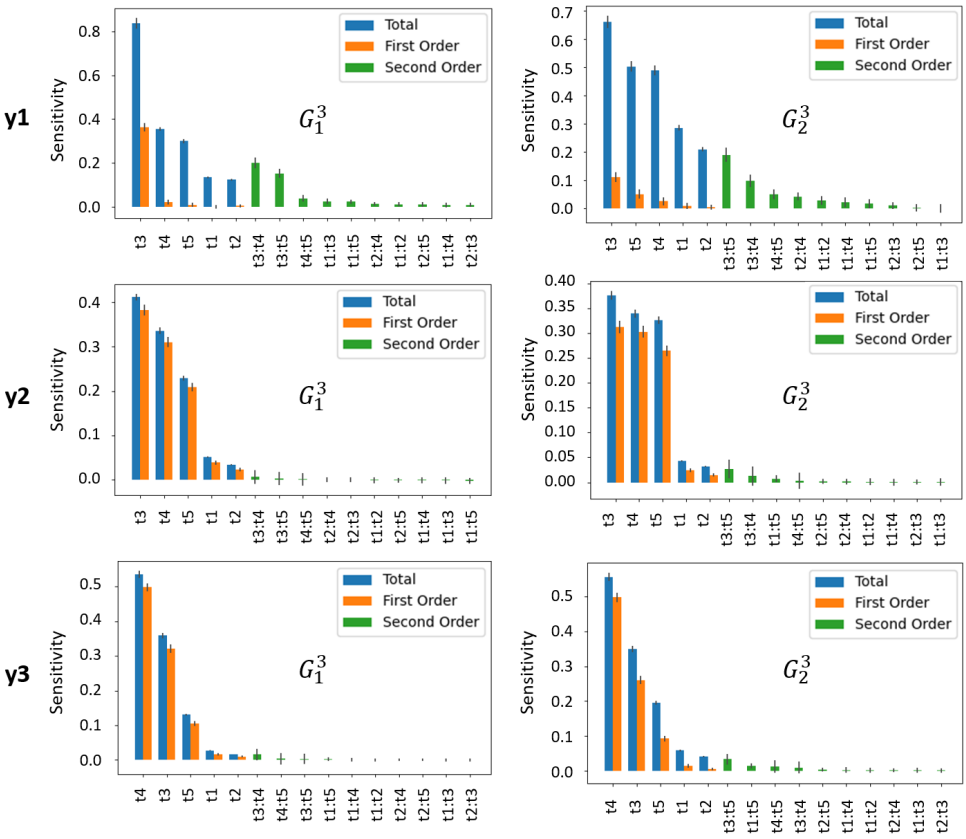

Figure 22: Effect of grid discretization on the order of ranking based on Sobol' indices for Case 3.

maximum packing, t4, while DP4 was sensitive to t4, exponential factor (t2) and pressure linear scale factor (t1) in the same order of ranking. In Case 3, interface height (y1), pressure drop across the riser (y2) and pressure drop across the standpipe (y3) were the QoIs. t3 is the most influential parameter for y1 while interaction between t3 and t5 is quite pronounced compared to their main effects. The most sensitive parameters for y2 were t4, t3 and t5 following the same order of ranking, while t4 was the most influential parameter for y3. Interaction effects appeared to be negligible for y2 and y3 in the range considered.

It was also observed that within a given domain, sensitivities of PIC parameters could vary depending on the local flow conditions. As seen in Cases 2 and 3, the influence of these variables changed between dense and dilute regions. In addition, this study enabled a preliminary understanding of parametric sensitivities to grid refinement. The order of importance ranking based on Sobol' indices was not preserved when the same sampling space was used at different grid levels. Instead, statistical weight (t3) was scaled based on grid volume to obtain better consistency in ranking. This approach is more in line with the flow physics for the following reasons: (i) maximum number of parcels in a cell becomes dependent only on t4 and (ii) volume

of parcel is restricted to avoid spurious interpolation operations. However, convergence was not demonstrated in all the cases considered and warrants further validation and quantitative analyses.

This study marks the first step to provide the MFiX-PIC user community with guidelines for selecting parameters backed by a rigorous statistics-based approach. The results obtained highlight the sensitivity of model parameters under different flow conditions as well as aid in designing simulation campaigns aimed at calibration, which will be pursued in the future. From a modeling standpoint, the study also highlighted the need for assessing performance of PIC parameters to model transition between dense and dilute regions which frequently occur in industrial applications.

Acknowledgment

This work was performed in support of the US Department of Energy's Fossil Energy Crosscutting Technology Research. The work was executed through the NETL Research and Innovation Center's Advanced Reactor Systems Program. Research performed by Leidos Research Support Team staff was conducted under the RSS contract 89243318CFE000003. The authors would also like to acknowledge the support of Justin Weber (NETL), the

lead developer of Nodeworks, in implementing several features used for the results presented.

Disclaimer

This work was funded by the Department of Energy, National Energy Technology Laboratory, an agency of the United States Government, through a support contract with Leidos Research Support Team (LRST).

References

[1] J. Musser, A. S. Almgren, W. D. Fullmer, O. Antepara, J. B. Bell, J. Blaschke, K. Gott, A. Myers, R. Porcu, D. Rangarajan, M. Rosso, W. Zhang, M. Syamlal, Mfix-exa: A path toward exascale cfd-dem simulations, The International Journal of High Performance Computing Applications 0 (0) 10943420211009293. URL: https://doi.org/10.1177/10943420211009293. doi:10.1177/10943420211009293. arXiv:https://doi.org/10.1177/10943420211009293.

[2] D. Rangarajan, J. S. Curtis, S. Benyahia, A. G. Mychkovsky, Continuum model validation of gas jet plume injection into a gas–solid bubbling fluidized bed, AIChE Journal 59 (2013) 3247–3264.

[3] D. Rangarajan, T. Shiozawa, Y. Shen, J. S. Curtis, A. Yu, Influence of operating parameters on raceway properties in a model blast furnace using a two-fluid model, Industrial & Engineering Chemistry Research 53 (2014) 4983–4990.

[4] J. E. Higham, M. Shahnam, A. Vaidheeswaran, Using a proper orthogonal decomposition to elucidate features in granular flows, Granular Matter 22 (2020) 86. doi:https://doi.org/10.1007/s10035-020-01037-7.

[5] J. E. Higham, M. Shahnam, A. Vaidheeswaran, Anomalous diffusion in a bench-scale pulsed fluidized bed, Physical Review E 103 (2021) 043103.

[6] L. Lu, J. Xu, W. Ge, Y. Yue, X. Liu, J. Li, Emms-based discrete particle method (emms–dpm) for simulation of gas–solid flows, Chemical Engineering Science 120 (2014) 67–87.

[7] L. Lu, A. Morris, T. Li, S. Benyahia, Extension of a coarse grained particle method to simulate heat transfer in fluidized beds, International Journal of Heat and Mass Transfer 111 (2017) 723–735.

[8] L. Lu, X. Gao, M. Shahnam, W. A. Rogers, Bridging particle and reactor scales in the simulation of biomass fast pyrolysis by coupling particle resolved simulation and coarse grained cfd-dem, Chemical Engineering Science 216 (2020) 115471.

[9] A. Di Renzo, E. S. Napolitano, F. P. Di Maio, Coarse-grain dem modelling in fluidized bed simulation: A review, Processes 9 (2021) 279.

[10] Snider, D.M., Three dimensional multiphase particle-in-cell model for dense particle flows, Journal of Computational Physics 170 (2001) 523–549.

[11] F. Li, F. Song, S. Benyahia, W. Wang, J. Li, Mp-pic simulation of cfb riser with emms-based drag model, Chemical Engineering Science 82 (2012) 104–113.

[12] F. H. Harlow, J. E. Welch, Numerical calculation of time-dependent viscous incompressible flow of fluid with free surface, The Physics of Fluids 8 (1965) 2182–2189. URL: https://aip.scitation.org/doi/abs/10.1063/1.1761178. doi:10.1063/1.1761178. arXiv:https://aip.scitation.org/doi/pdf/10.1063/1.1761178.

[13] M. Andrews, P. O'Rourke, The multiphase particle-in-cell (mp-pic) method for dense particulate flows, International Journal of Multiphase Flow 22 (1996) 379 – 402. URL: http://www.sciencedirect.com/science/article/pii/0301932295000720. doi:https://doi.org/10.1016/0301-9322(95)00072-0.

[14] D. Snider, P. O'Rourke, M. Andrews, An incompressible two-dimensional multiphase particle-in-cell model for dense particle flows, Technical Report, Los Alamos National Laboratory, Los Alamos, NM (United States), 1997. doi:10.2172/4769185.

[15] P. J. O'Rourke, P. P. Zhao, D. Snider, A model for col-

lisional exchange in gas/liquid/solid fluidized beds, Chemical Engineering Science 64 (2009) 1784 – 1797. URL: http://www.sciencedirect.com/science/article/pii/S0009250908006829. doi:https://doi.org/10.1016/j.ces.2008.12.014.

[16] P. J. O'Rourke, D. M. Snider, An improved collision damping time for mp-pic calculations of dense particle flows with applications to polydisperse sedimenting beds and colliding particle jets, Chemical Engineering Science 65 (2010) 6014 – 6028. URL: http://www.sciencedirect.com/science/article/pii/S0009250910005075. doi:https://doi.org/10.1016/j.ces.2010.08.032.

[17] P. J. O'Rourke, D. M. Snider, Inclusion of collisional return-to-isotropy in the mp-pic method, Chemical Engineering Science 80 (2012) 39 – 54. URL: http://www.sciencedirect.com/science/article/pii/S0009250912003284. doi:https://doi.org/10.1016/j.ces.2012.05.047.

[18] P. J. O'Rourke, D. M. Snider, A new blended acceleration model for the particle contact forces induced by an interstitial fluid in dense particle/fluid flows, Powder Technology 256 (2014) 39 – 51. URL:

http://www.sciencedirect.com/science/article/pii/S003259101400103X. doi:https://doi.org/10.1016/j.powtec.2014.01.084.

[19] Clarke, MaryAnn and Musser, Jordan, The MFiX Particle-in-Cell Method (MFiX-PIC) Theory Guide, NETL TRS Report NETL-TRS-2020/2115, NETL, 2020. doi:10.2172/1630414.

[20] A. Vaidheeswaran, J. Musser, M. A. Clarke, Verification and Validation of MFiX-PIC, NETL TRS Report NETL-TRS-2-2020, NETL, 2020.

[21] T. Kadyrov, F. Li, W. Wang, Impacts of solid stress model on mp-pic simulation of a cfb riser with emms drag, Powder Technology 354 (2019) 517–528.

[22] Y. Jiang, F. Li, W. Ge, W. Wang, Emms-based solid stress model for the multiphase particle-in-cell method, Powder Technology 360 (2020) 1377–1387.

[23] A. Gel, A. Vaidheeswaran, J. Musser, C. H. Tong, Toward the development of a verification, validation, and uncertainty quantification framework for granular and multiphase flows part 1: Screening study and sensitivity analysis, Journal of Verification, Validation and Uncertainty Quantification 3 (2018).

[24] A. Gel, A. Vaidheeswaran, M. A. Clarke, Deterministic Calibration of MFiX-PIC, Part 1: Settling Bed, NETL TRS Report NETL-TRS-XX-2020 (under review), NETL, 2020.

[25] M. A. Clarke, J. Musser, The mfix particle-in-cell method (mfix-pic) theory guide (2020). doi:10.2172/1630414.

[26] W. Dexter, D. Tanner, Packing densities of mixtures of spheres with log-normal size distributions, Nature Physical Science 238 (1972) 31–32. URL: https://doi.org/10.1038/physci238031a0.

[27] D. M. Thies-Weesie, A. P. Philipse, Liquid permeation of bidisperse colloidal hard-sphere packings and the kozeny-carman scaling relation, Journal of Colloid and Interface Science 162 (1994) 470 – 480. URL: http://www.sciencedirect.com/science/article/pii/S0021979784710629. doi:https://doi.org/10.1006/jcis.1994.1062.

[28] K. W. Desmond, E. R. Weeks, Influence of particle size distribution on random close packing of spheres, Phys. Rev. E 90 (2014) 022204. URL: https://link.aps.org/doi/10.1103/PhysRevE.90.022204. doi:10.1103/PhysRevE.90.022204.

[29] W. Nan, Y. Wang, Y. Liu, H. Tang, Dem sim-

ulation of the packing of rodlike particles, Advanced Powder Technology 26 (2015) 527 – 536. URL: http://www.sciencedirect.com/science/article/pii/S0921883114003264. doi:https://doi.org/10.1016/j.apt.2014.12.012.

[30] T. Tsunoyama, M. Yoshida, A. Shimosaka, Y. Shirakawa, Effects of mixing ratio and order of admixed particles with two diameters on improvement of compacted packing fraction, Advanced Powder Technology 31 (2020) 2430 – 2437. URL: http://www.sciencedirect.com/science/article/pii/S0921883120301278. doi:https://doi.org/10.1016/j.apt.2020.04.005.

[31] A. Vaidheeswaran, A. Gel, M. A. Clarke, W. Rogers, Sensitivity Analysis of Particle-In-Cell Modeling Parameters in Settling Bed, Bubbling Fluidized Bed and Circulating Fluidized Bed, NETL Technical Report Series DOE.NETL-2021.2642, NETL, 2021. doi:10.2172/1756845.

[32] R. Jin, W. Chen, A. Sudjianto, An efficient algorithm for constructing optimal design of computer experiments, Journal of Statistical Planning and Inference 134 (2005) 268 – 287. URL:

http://www.sciencedirect.com/science/article/pii/S0378375804001922. doi:https://doi.org/10.1016/j.jspi.2004.02.014.

[33] A. Vaidheeswaran, C. Li, H. Ashfaq, X. Wu, S. Rowan, W. Rogers, Data from experiments on bubbling fluidization of group b glass particles, 2020. doi:10.26434/chemrxiv.12690104.v1.

[34] A. Vaidheeswaran, S. Rowan, Chaos and recurrence analyses of pressure signals from bubbling fluidized beds, Chaos, Solitons & Fractals (2020) 110354. URL: http://www.sciencedirect.com/science/article/pii/S0960077920307499. doi:https://doi.org/10.1016/j.chaos.2020.110354.

[35] Y. Xu, J. Musser, T. Li, B. Gopalan, R. Panday, J. Tucker, G. Breault, M. A. Clarke, W. A. Rogers, Numerical simulation and experimental study of the gas-solid flow behavior inside a full-loop circulating fluidized bed: Evaluation of different drag models, Industrial & Engineering Chemistry Research 57 (2018) 740–750. URL: https://doi.org/10.1021/acs.iecr.7b03817. doi:10.1021/acs.iecr.7b03817. arXiv:https://doi.org/10.1021/acs.iecr.7b03817.

[36] National Energy Technology Laboratory (NETL), Nodeworks,

2020. URL: https://mfix.netl.doe.gov/nodeworks, URL: https://mfix.netl.doe.gov/nodeworks.

[37] National Energy Technology Laboratory (NETL), MFiX-PIC, 2020. URL: https://mfix.netl.doe.gov/mfix/mfix-documentation/, URL: https://mfix.netl.doe.gov/mfix/mfix-documentation/.

[38] I. M. Sobol, Global sensitivity indices for nonlinear mathematical models and their monte carlo estimates, Mathematics and computers in simulation 55 (2001) 271–280.

[39] C. J. Freitas, Standards and Methods for Verification, Validation, and Uncertainty Assessments in Modeling and Simulation, Journal of Verification, Validation and Uncertainty Quantification 5 (2020).